Detection of the Direct Effect of Clay on Polymer Dynamics: The Case of Spin-Labeled Poly(methyl acrylate)/Clay Nanocomposites Studied by ESR, XRD, and DSC

Yohei Miwa,[†] Andrew R. Drews,[‡] and Shulamith Schlick*,[†]

Department of Chemistry and Biochemistry, University of Detroit Mercy, 4001 West McNichols Road, Detroit, Michigan 48221-3038, and Ford Research and Innovation Center, Ford Motor Company, MD 3182, P.O. Box 2053, Dearborn, Michigan 48121

Received January 13, 2006; Revised Manuscript Received March 8, 2006

ABSTRACT: Nanocomposites of poly(methyl acrylate) (PMA) with synthetic fluoromica (Somasif) as the inorganic component were studied as a function of clay content by the spin-label electron spin resonance (ESR) technique, X-ray diffraction (XRD), and differential scanning calorimetry (DSC). PMA was modified by attachment of nitroxide radicals and trimethylammonium chloride (TMC) groups in low concentrations ($\approx$ 1 mol %). Ion exchange between the TMC moieties as anchoring groups and the Somasif surface allowed the preparation of exfoliated nanocomposites even in the absence of surfactants. The presence of nitroxide labels and the absence of surfactants allowed the detection of the direct effect of the clay on polymer dynamics. The properties of these materials were compared with those of the nanocomposites prepared with the clay modified by surfactants. Structural data from XRD were combined with ESR results in order to assess the extent and intensity of polymer−clay interactions at the interface. ESR spectra indicated that the mobility of PMA chains in the nanocomposites is constrained due to the interactions in the interface region. The average thickness of the rigid interface in the nanocomposites prepared without surfactants was estimated to be in the range 5−15 nm, based on the deconvolution of ESR spectra measured as a function of temperature into slow (S) and fast (F) components. The average interface thickness decreased with increasing Somasif content, most likely because of overlap between Somasif platelets. In nanocomposites prepared in the presence of surfactants, the interaction between PMA and Somasif was reduced, and the mobility of PMA was enhanced. No significant effect on polymer dynamics was detected in conventional composites, in which the clay was dispersed on a scale siginificantly larger than the nanoscale.

Introduction

Polymer/clay nanocomposites, formed by dispersing nanosized clay particles in a polymer matrix, have received much attention in both scientific and industrial fields due to their enhanced mechanical properties and thermal stability, even at low inorganic content, 2−5 wt %.[1,2] Two main types of polymer/clay nanocomposites are usually studied: *intercalated*, in which polymer chains occupy the interlayer spaces between staking silicate platelets, and d*elaminated* or *exfoliated*, in which discrete clay layers are dispersed in the polymer matrix. As expected, the type of clay dispersion in the polymer matrix has a major impact on the polymer properties in the nanocomposites. Exfoliated nanocomposites are usually more desirable because the strong interactions between the polymer and the clay layers can lead to controllable and often optimized polymer properties. Transmission electron microscopy and X-ray diffraction (XRD) are typical methods used to estimate the structure of polymer/clay nanocomposites.[1,2] XRD measures the distance between the platelets in the neat clay and the changes that result from polymer intercalation between the silicate layers.

Polymer segmental mobility is one of the most important factors affecting thermoplastic flow, gas diffusion, and ion transport in polymer/clay systems. The effect of clays on the segmental motion expressed as the glass transition, T_g, of polymers in nanocomposites has been evaluated as a possible indicator of this effect. However, information from the measurement of T_g of polymers in nanocomposites is not always conducive to a better understanding of the system. While some papers claimed that no change in T_g was detected,[3] others reported an increase in T_g[4−9] or even the total disappearance of the transition;[10,11] in other cases, a decrease of the T_g for nanocomposites was reported.[12−15]

Nanocomposites have significantly larger interfacial area between the matrix polymer and the clay compared to conventional composites. This increase in interfacial area results in an interfacial region where the polymer matrix is expected to have properties that are significantly different compared to the bulk polymers. Therefore, the study of molecular motion of polymers at the interface is critical for an understanding of the effects of clays on polymer properties.

If surfactants are added to enhance the miscibility between the two components, the nature of the interface as well as the polymer dynamics may be affected. This surfactant effect is considered to be one of the reasons why contradictory conclusions about the T_g of polymers in composites have often been reported. The T_g measured by DSC of syndiotactic poly(methyl methacrylate) (s-PMMA) confined between layers of an organophilic montmorillonite (OMMT) increased with an increase in OMMT content; this increase was interpreted in terms of an increase in intermolecular carbonyl group interaction.[9] A decrease of T_g was, however, reported for epoxy/OMMT systems and attributed to the formation of an interphase in which surfactant molecules attached to the silicate surface plasticize the intercalated polymer.[16,17]

Electron spin resonance (ESR) spin-label and spin-probe techniques allow us to discern different sites in complex systems and can provide information on the local dynamics on time scales in the range 10^{-11}−10^{-7} s and length scale of a few

[†] University of Detroit Mercy.
[‡] Ford Research and Innovation Center, Ford Motor Company.
* Corresponding author. E-mail: schlicks@udmercy.edu.

10.1021/ma0600963 CCC: $33.50
Published on Web 03/30/2006

Chart 1

(A) [2-(acryloyloxy)ethyl]trimethylammonium chloride (2ATAC)

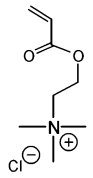

(B) Spin-labeled PMA with attached trimethylammonium chloride groups

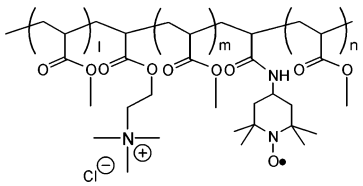

(C) Surfactant in modified MEE, methyl tallow bis-2-hydroxyethylammonium

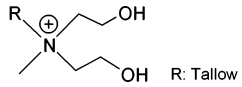

nanometers.[18] In nanocomposites, these methods have the potential to reveal the effect of surfactants and clay surface on the polymer dynamics and to complement studies that focus on average system properties. An ESR study of polymer/clay composites was recently reported by Jeschke et al.,[18] in a study of surfactants in organoclays and their composites with polystyrene (PS), using several ESR techniques: ESR of the spin probe, electron nuclear double resonance (ENDOR), electron spin echo envelope modulation (ESEEM), and four-pulse double electron−electron resonance (DEER). The spin probe was the surfactant (*N*,*N*,*N*-trimethyl-*N*-hexadecylammonium ions) labeled with nitroxides at the α or *ω* ends. The variation of the ESR spectra with temperature showed that the mobility of the anchor point on the clay surface was much lower than that of the free tail. This technique allowed the determination of surfactant mobility in the nanocomposites: As PS ($M_n = 10\,000$) was blended with the organoclay, the mobility of the surfactants was significantly reduced. DEER and X-ray scattering experiments were interpreted in terms of PS intercalation in the clay.

We present a study of the molecular mobility of poly(methyl acrylate) (PMA) in nanocomposites with synthetic fluoromica (Somasif ME100), based primarily on spin-label ESR. The polymer was modified by attached trimethylammonium chloride and stable nitroxide radical groups at low concentration (≈ 1 mol %), as shown in Chart 1. PMA/Somasif nanocomposites were prepared via ion exchange between the trimethylammonium chloride moieties in the PMA chain and the Somasif surface; this technique allowed the preparation of nanocomposites without surfactants. The focus was on direct observation by ESR of the influence of the Somasif surface on the segmental dynamics of PMA chains and of the length scale of the Somasif effect. Additional details were obtained by XRD and DSC.

Experimental Section

Materials. Methyl acrylate (MA, 99%), *tert*-butyl acrylate (*t*BA, 98%), 2,2′-azobis(2-methylpropionitrile) (AIBN, 98%), [2-(acryloyloxy)ethyl]trimethylammonium chloride solution (2ATAC, 80 wt % in water), deionized water (CHROMASOLV), 2,2,6,6-tetramethyl-4-aminopiperidine-1-oxyl (4-amino-TEMPO, 99%), toluene (99.5%), methanol (99.8%), and acetone (99.5%) were purchased from Aldrich and used as received. *N*,*N*-Dimethylformamide (DMF, 99.9%, Fisher Scientific) and chloroform (99%, Fisher Scientific) were used without further purification. Inhibitors in MA and *t*BA were adsorbed on activated aluminum oxide (150 mesh, Aldrich) and removed.

Synthetic Somasif (ME-100) and Somasif MEE (MEE) were supplied by CO-OP Chemical Co., Ltd., Japan. The chemical composition and the cationic exchange capacity of Somasif are $Na_{0.66}Mg_{2.68}(Si_{3.98}Al_{0.02})O_{10.02}F_{1.96}$ and 115 mequiv/g, respectively.[19] MEE is Somasif modified with the surfactant methyl tallow bis-(2-hydroxyethyl)ammonium (Chart 1).[19,20]

Synthesis of Spin-Labeled PMA. Methyl acrylate (MA) was polymerized via radical polymerization in DMF solution. The initial molar composition was MA:*t*BA:2ATAC:AIBN = 100:1:1:0.3. The reaction mixture was stirred for 30 min under N_2 flow, and the polymerization was carried out at 343 K for 6 h. The mixture was then dissolved in acetone and precipitated in a water/methanol mixture, and the precipitate was dried in a vacuum oven at 353 K for 24 h. As a result, PMA containing *tert*-butyl and trimethylammonium chloride moieties along the chain was prepared. For spin-labeling, an amide−ester interchange reaction between the *tert*-butyl moiety and 4-amino-TEMPO was carried out in acetone solution at 283 K for 4 days, followed by PMA precipitation in a water/methanol mixture to remove the large amount of unreacted spin probe and drying in a vacuum at 353 K for 24 h. This precipitation was repeated four times, and the ESR signal from the probe was measured in the solution; after the fourth precipitation the signal from the probe was not detected, indicating complete removal of unreacted 4-amino-TEMPO. The chemical structure of spin-labeled PMA containing trimethylammonium chloride moieties is shown in Chart 1. The weight-average molecular weight (M_w) and the molecular weight distribution (M_w/M_n) of this sample were 11 600 and 1.57, respectively, as determined by gel permeation chromatography (GPC) using PS standards (Tosoh).

Preparation of PMA/Somasif Nanocomposites. Somasif was dispersed in deionized water to a concentration of 1.5 wt %. The dispersion was ultrasonicated and stirred until a homogeneous system was observed, usually 1−3 h. Methanol was then added, and the mixture was stirred for 1 h; the methanol/water ratio (v/v) was five. The spin-labeled PMA was dissolved at 323 K in methanol to a concentration of 5 wt %. After the PMA was completely dissolved, deionized water was added (to 13 vol %), and the solution was stirred for 30 min at 323 K. This solution was added to the Somasif dispersion, and the mixture was vigorously stirred at 323 K for 6 h, followed by solvent evaporation in the hood. The sample was then dried in a vacuum oven at 353 K for 12 h.

Preparation of PMA/Somasif Conventional Composites. Somasif (89 mg) was dispersed in 30 mL of chloroform and ultrasonicated for 4 h. PMA (500 mg) was dissolved in 15 mL of acetone, and the solution was added to the Somasif dispersion and stirred for 6 h. The solvent was then evaporated in the hood, and the sample was dried in a vacuum oven at 353 K for 12 h.

Preparation of PMA/MEE Nanocomposites. MEE (120 mg) was dissolved in 30 mL of chloroform and ultrasonicated for 4 h. PMA (469 mg) was dissolved in 15 mL of acetone, and the solution was added to the MEE solution and stirred for 6 h. The solvent was then evaporated in the hood, and the sample was afterward dried in a vacuum oven at 353 K for 12 h.

As demonstrated below, the type of composite was determined by ESR and XRD. The term "composites" refers to materials in which the dispersion of the clay is on a scale significantly larger that the nanoscale. The notation we use for the various types of composites is SP*n* for nanocomposites based on Somasif, COMP*n* for composites based on Somasif, and MEEP*n* for nanocomposites based on MEE (modified Somasif), where *n* is the wt % clay.

ESR Measurements. Spectra were recorded with Bruker X-band EMX spectrometers operating at 9.7 GHz with 100 kHz magnetic field modulation and equipped with the Acquisit 32 Bit WINEPR data system version 3.01 for acquisition and manipulation and the ER4111VT variable temperature unit. The microwave frequency was measured with a Hewlett-Packard 5350B microwave frequency counter. Most spectra were collected with the following parameters: sweep width 150 G, microwave power 2 mW, time constant 20.48 ms, conversion time 40.96 ms, 2−9 scans, and 2048 points.

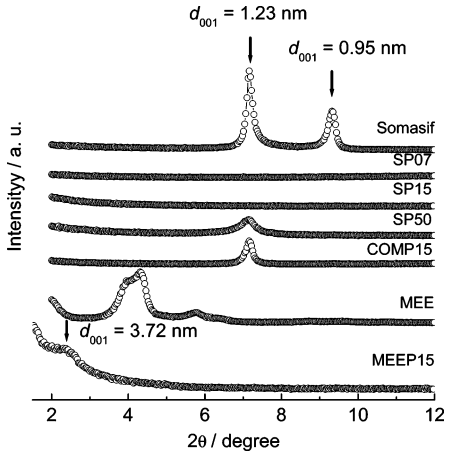

Figure 1. XRD patterns of Somasif, SP07, SP15, SP50, and COMP15, MEE, and MEEP15.

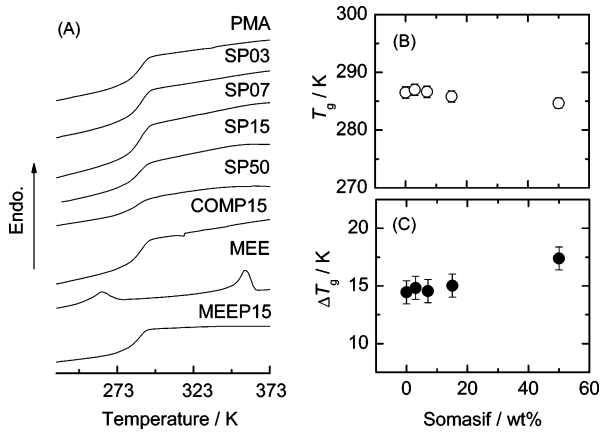

Figure 2. (A) DSC traces for the indicated systems. (B) T_g and (C) ΔT_g values for PMA and SP*n* nanocomposites as a function of Somasif content.

The modulation amplitude was varied in the range 1−3 G, depending on the line width. The temperature was controlled within ±1 K. All samples were allowed to equilibrate for at least 10 min after reaching the desired temperature.

Simulation of ESR Spectra. Rigid-limit ESR spectra were calculated with a simulation software based on the stochastic Liouville equation.[21] The simulated spectra were fitted to the experimental spectra using a PC version of the NLSL program based on a modified Levenberg−Marquart minimization algorithm, which iterates the simulations until a minimum least-squares fit to experiment is reached.[22] The *A* and *g* tensors were determined by analyzing rigid-limit spectra of samples. Very slow isotropic Brownian rotational diffusion of the spin-label was chosen as the model, and the fitted parameters were the *A* and *g* tensor components and the line widths. Identical principal axes systems for both tensors were assumed.

Differential Scanning Calorimetry (DSC). Thermal analysis was carried out using a Q10 differential scanning calorimeter manufactured by TA Instruments calibrated with an indium standard. Cooling was accomplished by a TA Instruments quench cooler accessory. The DSC cell was purged with dry nitrogen flowing at a rate of 50 mL/min. Samples were heated from ambient temperature to about T_g + 100 K at a rate of 20 K/min, held for 5 min, and cooled at a rate of 10 K/min. Data collection was carried out on cooling.

X-ray Diffraction (XRD). Measurements were performed on a Scintag X2 diffractometer using Cu Kα radiation generated at 45 kV and 40 mA. Samples were scanned at 0.03°/s in the range of $2\theta = 2-12°$ using a step size of 0.03°. The Bragg equation was applied to calculate the *d* spacing of the Somasif platelets.

Gel Permeation Chromatography (GPC). GPC was carried out in Nagoya, Japan, under the following conditions: in THF (1 mL/min) at 313 K on four polystyrene gel columns (Tosoh TSK gel GMH (bead size is 7 μm) and G4000H, G2000H, and G1000H (5 μm)) that were connected to a Tosoh CCPE (Tosoh) pump and an ERC-7522 RI refractive index detector (ERMA Inc.). The columns were calibrated against standard PS (Tosoh) samples.

Results

XRD plots for Somasif, SP07, SP15, SP50, and COMP15 measured at ambient temperature are shown in Figure 1. The neat clay has two peaks, at $2\theta = 7.2°$ ($d_{001} = 1.23$ nm) and 9.3° (0.95 nm). These peaks are absent in the SP07 and SP15 samples. Both SP50 and COMP15 samples exhibit the diffraction peak at $2\theta = 7.2°$; the half-height widths of the peak are 0.2°, 0.5°, and 0.2° for neat Somasif, SP50, and COMP15, respectively.

XRD patterns for MEE and MEEP15 are also shown in Figure 1. The MEE peaks are at $2\theta = 4.0°$ ($d_{001} = 2.15$ nm), 4.3° (2.05 nm), 5.8° (1.53 nm), and 6.4° (1.39 nm). The d_{001} of the MEE is larger than that of Somasif because of structure modification by surfactants. The MEEP15 sample has only one peak at $2\theta = 2.4°$ ($d_{001} = 3.72$ nm).

Table 1. Characteristics of Samples

sample	Somasif (wt %)	T_g (K)[a]	ΔT_g (K)[a]	structure[b]
PMA		287 ± 1	14 ± 1	
SP03	3	287 ± 1	15 ± 1	
SP07	7	287 ± 1	15 ± 1	exfoliated
SP15	15	286 ± 1	15 ± 1	exfoliated
SP50	50	285 ± 1	17 ± 1	partially exfoliated
COMP15	15	287 ± 1	14 ± 1	composite
MEEP15	15	285 ± 1	14 ± 1	intercalated

[a] Determined by DSC. [b] Estimated by XRD.

DSC traces of the indicated samples are shown in Figure 2A. Corresponding T_g values and widths of the transition, ΔT_g, of the SP*n* nanocomposites are plotted as a function of Somasif content in parts B and C of Figure 2, respectively. T_g was defined as the temperature at the midpoint of the glass transition step, i.e., the temperature corresponding to half-height of the endothermic shift, and ΔT_g is the separation between onset and end temperatures.[23] The T_g and ΔT_g values are listed in Table 1. T_g values did not vary significantly with Somasif content, but ΔT_g of SP50 was larger than that of PMA. MEE showed crystallizations peaks for surfactants at 263 and 357 K. MEEP15 showed a glass transition at 285 K, but no crystallization peaks; the disappearance of these peaks indicates that surfactant crystallization was prevented, most likely due to intercalation of PMA.

ESR Measurements. ESR spectra measured at 100 K and corresponding simulated spectra are shown in Figure 3A. The values of the parallel and perpendicular line widths ($\Delta H_{||}$ and $\Delta H_{\perp}$) and the *A* and *g* tensors used for fitting are listed in Table 2. The principal values of the *A* and *g* tensors do not vary significantly with Somasif content, with the exception of $2A_{zz}$, which is larger in SP50, as seen in Figure 3B. The line widths of the parallel and perpendicular components, $\Delta H_{||}$ and $\Delta H_{\perp}$, increase with increasing Somasif content.

Selected ESR spectra of spin-labeled PMA, SP15, and MEEP15 in the temperature range 100−400 K are shown in parts A, B, and C of Figure 4, respectively. The extreme separation (ES) given on the left of the spectra was read from vertically expanded spectra, with a maximum error margin of ±0.5 G. The dotted vertical lines indicate the values of $2a_N$, twice the isotropic hyperfine splittings from ^{14}N; these values

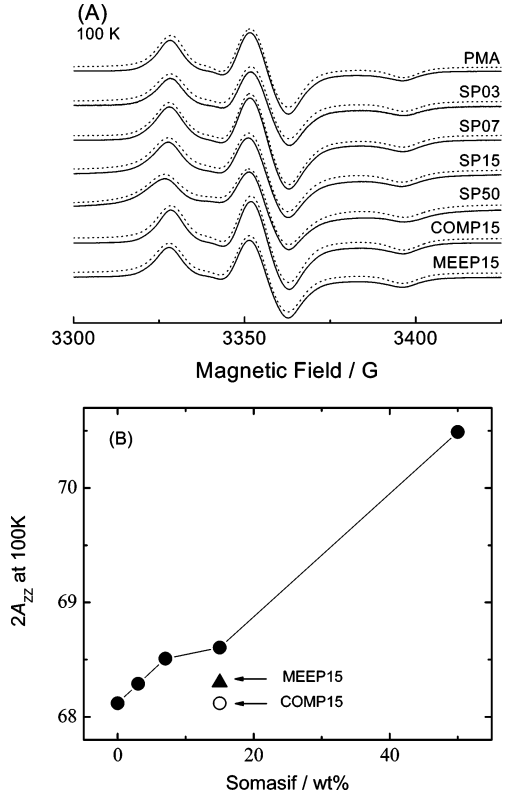

Figure 3. (A) Experimental (solid lines) and simulated (dotted lines) ESR spectra at 100 K for the indicated systems. (B) Plot of the extreme separation at 100 K, $2A_{zz}$, for SP*n* nanocomposites (●), COMP15 (○), and MEEP15 (▲) as a function of Somasif content.

Table 2. Parameters Used for the Simulation of ESR Spectra at 100 K

sample	g_{xx}	g_{yy}	g_{zz}	A_{xx} (G)	A_{yy} (G)	A_{zz} (G)	$\Delta H_{\perp}$ (G)	$\Delta H_{\parallel}$ (G)
PMA	2.0100	2.0063	2.0021	7.0	5.7	34.0	1.9	3.4
SP03	2.0099	2.0063	2.0023	7.0	5.5	34.2	2.2	3.6
SP07	2.0100	2.0065	2.0024	7.2	5.4	34.3	2.5	4.1
SP15	2.0098	2.0063	2.0024	7.3	5.4	34.3	3.8	5.2
SP50	2.0096	2.0061	2.0025	7.1	5.4	35.3	5.8	7.1
COMP15	2.0099	2.0064	2.0023	7.0	5.5	34.1	2.1	3.6
MEEP15	2.0099	2.0064	2.0023	7.1	5.5	34.1	2.3	3.7

are 31.1, 30.8, and 31.2 G for PMA, SP15, and MEEP15, respectively. The temperature dependence of the spectra is due to changes in the rotational rate of the nitroxide radical, characterized by the correlation time, τ_c. The two motional regimes usually detected in ESR experiments correspond to slow-motional spectra, with correlation times in the range of $10^{-7}-10^{-9}$ s, and fast-motional spectra, with τ_c in the range $10^{-9}-10^{-11}$ s. The rigid limit spectrum of PMA at 100 K changed as the temperature increased, and at 400 K the typical fast-motional spectrum appears. At the same temperature, two components, slow and fast, are detected for SP15.

A plot of the extreme separation (ES) as a function of temperature is a visual indicator of local dynamics. Plots for PMA and the SP*n* nanocomposites are presented in Figure 5A and for SP15, COMP15, and MEEP15 in Figure 5B. The ES decreased with increase of temperature, and the smallest decrease was detected for SP50. Above ≈350 K, the ES values of COMP15 were significantly lower than those of SP15, even though these samples contained the same amount of the Somasif; ES values of MEEP15 and SP15 are similar.

ESR spectra at 400 K are shown in Figure 6; all spectra, with the exception of PMA, consist of fast and slow components. The relative intensities of the two spectral components were

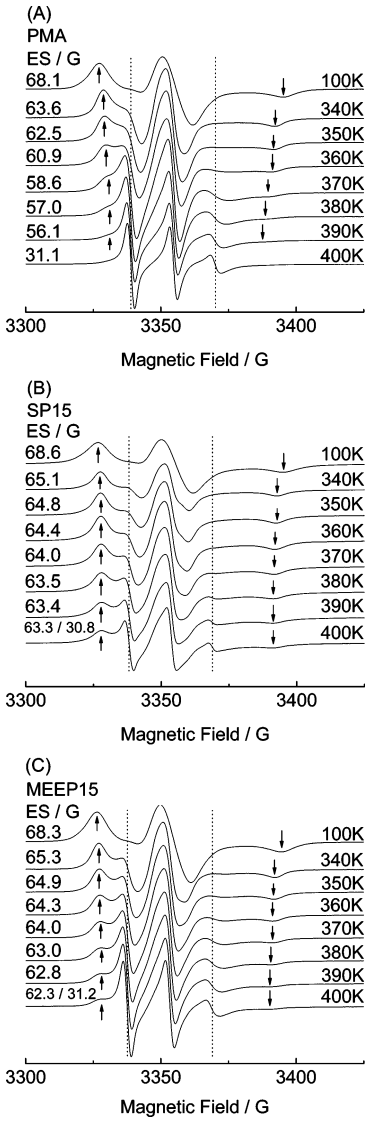

Figure 4. Temperature variation of ESR spectra for PMA (A), SP15 (B), and MEEP15 (C). The extreme separation (ES) is indicated by arrows and given on the left. The $2a_N$ value is indicated in each set of spectra by dotted lines and given for $T = 400$ K.

deduced by spectral deconvolution: For example, the ESR spectra of the SP15 measured at 380 and 385 K had almost the same ES values, but the intensities of the fast and slow components were different. Therefore, the spectrum of the slow component was obtained by subtraction of the spectrum measured at 385 K from that measured at 380 K. In the second step, the slow component was subtracted from the spectrum measured at 400 K in order to isolate the fast component, as the ES values of the slow component measured above 380 K were comparable. Similar procedures were carried out to calculate the relative intensity of the fast and slow components for the other samples; the relative intensity of the slow component in percent is shown in Figure 6 for $T = 400$ K and in Table 3 for the temperature range 380−400 K. For the SP*n* nanocomposites, % slow increased with increasing Somasif content. In COMP15 and MEEP15, % slow values were much lower than those in SP15.

ESR spectra of SP50 at 340, 370, and 395 K are shown in Figure 7. Outermost peaks in the spectra measured at 340 and 370 K exhibit shoulders, which are indicated by arrows; the intensity of the shoulders increased with increasing temperature. Such shoulders were observed only for SP50.

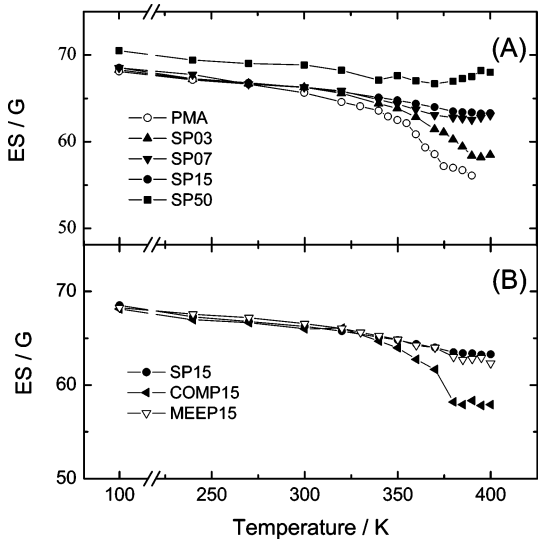

Figure 5. Temperature variation of the extreme separation (ES) for the indicated systems.

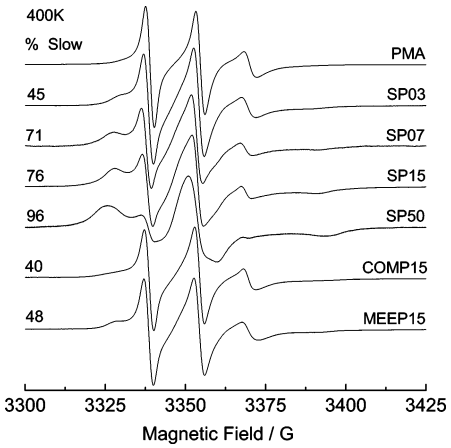

Figure 6. ESR spectra for the indicated systems measured at 400 K. The relative intensity of the slow component in % is given on the left. See text.

Table 3. Percentage of Slow Component[a]

temp (K)	SP03	SP07	SP15	SP50	COMP15	MEEP15
380		81	89		52	69
385		75	83		52	63
390	45	73	77	97	44	58
395	43	71	76	96	44	50
400	45	71	76	96	40	48

[a] With a margin error of ±2.

Discussion

Structure of Composites. As seen in Figure 1, Somasif exhibits two diffraction peaks, at $2\theta = 7.2°$ ($d_{001} = 1.23$ nm) and 9.3° (0.95 nm) (Figure 1). The distance of 1.23 nm is in good agreement with that reported by Maiti.[24] Chen et al. reported that the d_{001} value of MMT was reduced from 1.23 nm to the thickness of platelets (≈0.98 nm) after heat treatment at 800 °C because of dehydration.[25] Similarly, the shorter distance, 0.95 nm, is taken as an indicator that the clay as received contained some dehydrated regions. The original Somasif peaks are not detected in SP07 and SP15, suggesting complete clay exfoliation and dispersion in the polymer matrix. XRD measurements were not carried out for SP03, but on the basis of results for SP07 and SP15, it is reasonable to assume that the exfoliated structure also exists in SP03.

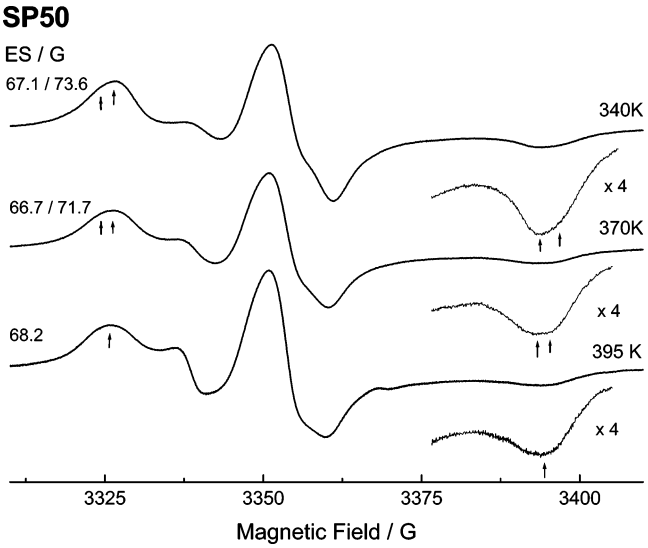

Figure 7. ESR spectra of SP50 measured at 340, 370, and 395 K. Shoulders at the extrema are shown with gray arrows. ES values of both spectral components are presented on the left.

The SP50 and the COMP15 samples show the diffraction peak at $2\theta = 7.2°$, indicating the presence of Somasif. On the basis of the analysis of ESR results discussed below, we concluded that SP50 consisted of both exfoliated and unexfoliated Somasif regions, due to the large amount of the Somasif loaded, and that COMP15 is a conventional composite, with Somasif platelets dispersed on a scale larger than nanoscale, possibly microscale.

As seen in Figure 1, d_{001} is larger for MEEP15 than for MEE, most likely because of PMA intercalation; additional proof for polymer intercalation in MEEP15 is the disappearance of the surfactant crystallization peaks observed by the DSC (Figure 2A).

Interactions at the PMA−Somasif Interface. The ESR line shapes measured as a function of temperature reflect both the local environment and the local dynamics. At 100 K the motion of the spin-labels is frozen, and the spectra reflect only the local environment and interactions.[26]

For the SP*n* nanocomposites, the $\Delta H_{||}$, $\Delta H_{\perp}$, and $2A_{zz}$ values (extreme separation measured in the rigid limit, at 100 K) increased with increasing Somasif content, as seen in Figure 3B and Table 2. The increase of A_{zz} indicates the location of the nitroxide label in the vicinity of the polar Somasif surface and an increased polymer−clay interaction with increasing Somasif content.[27] A similar increase of A_{zz} was detected in a recent study of spin-labeled polymer chains grafted or adsorbed on silica surfaces.[28,29]

The increase of $\Delta H_{||}$ and $\Delta H_{\perp}$ values with increasing Somasif content is assigned to a distribution of sites for the spin-labels, leading to a superposition of signals from multiple domains with a range of polarities: spin-labels located closer to the Somasif surface are strongly affected and show a larger extreme separation (ES) compared to spin-labels located at more distant sites. This conclusion is supported by the spectra for SP50 in Figure 7, which show shoulders at outermost peaks. These shoulders clearly reflect a distributions of nitroxides sites that differ in the local polarity and intensity of local interactions. The temperature variation of the extreme features brought into evidence sites with limited mobility that interact strongly with the clay and have a larger extreme separation, 71.7 and 73. 6 G, compared to ≈67−68 G for the more mobile sites. Similar shoulders at the extreme features were observed in other

heterogeneous systems. In the ESR spectra of spin probes in poly(ethylene-*ran*-methacrylic acid) (EMAA) ionomers, the shoulders were assigned to a superposition of ESR spectra of spin-probes located in the rigid ionic cluster phase and in the more mobile matrix phase.[30]

The $2A_{zz}$, $\Delta H_{||}$, and $\Delta H_{\perp}$ values of COMP15 and MEEP15 are lower than those of SP15, indicating a weaker polarity effect of the Somasif surface. In MEEP15 the polymer−clay interaction is prevented by the presence of the nonpolar alkyl surfactants chains; the surfactants act as a buffer and the polarity effect of the Somasif surface is weakened. In COMP15, this result is considered to reflect dispersion of the clay on a larger than nanoscale, leading to a smaller interfacial area. This conclusion provides the rationale for the appearance of the diffraction peak (Figure 1) for COMP15.

Restricted Molecular Motion in the Interfacial Region. As seen by comparing the three sets of spectra shown in Figure 4, the mobility of PMA is considerably restrained by the presence of Somasif: At 400 K the ESR spectrum of PMA is in the motionally narrowed regime (fast component), but that of SP15 consists of two components, and the relative intensity of the slow component is 76% (Table 3). The restricted molecular motion is caused primarily by attachment of trimethylammonium groups on the Somasif surface and additionally by the polar interaction between the ester groups and the siloxane oxygen on the basal surfaces of the silicate layers, as reported for the interaction between poly(ϵ-caprolactone) and clay.[31] The "anchoring" effect on a solid surface is expected not only to constrain the motion but also to increase the thickness of the restricted interfacial layer.[32] Moreover, the density of the polymer is expected to increase in the vicinity of the Somasif surface, leading to a lower polymer mobility.[33] We have also observed restricted mobility of spin-labeled PMA in nanocomposites prepared with montmorillonite (MMT) as the inorganic component instead of Somasif; this result is reasonable because the two clays are structurally similar. A detailed analysis of ESR spectra was, however, difficult, as the strong ESR signal of paramagnetic Fe(III), present in the basal structure of the MMT, significantly perturbed the ESR spectra of the spin-labeled guest.[34] Restricted mobility at the polymer−inorganic interface was also detected in poly(ethylene oxide)/silica particle nanocomposites by the ESR technique.[35]

The effect of Somasif content on polymer dynamics is clearly seen in the temperature variation of the ES (Figure 5A): At a given temperature the ES of the slow component increased with Somasif content, indicating increased interactions at the interface polymer−clay. This increase is contrary to the expectation that the constraining effect be independent of Somasif content, provided that the clay platelets are well separated. This increase may be due to overlap of interfacial regions of different platelets with an increase in the Somasif content, as shown in Figure 8: Polymer chains in interfacial regions confined by two or more Somasif platelets have lower mobility than those restricted by one platelet only. In addition, TMC groups can act as cross-linkers between Somasif platelets, leading to more proximity between Somasif platelets. In addition, higher Somasif content may shift the distribution of extreme separations to higher values.

In contrast to chains at the polymer−clay interface, the $2a_N$ values, of the fast component in the nanocomposites, are comparable to those in neat PMA (Figure 4), indicating a constant polymer mobility in regions distant from the Somasif surface.

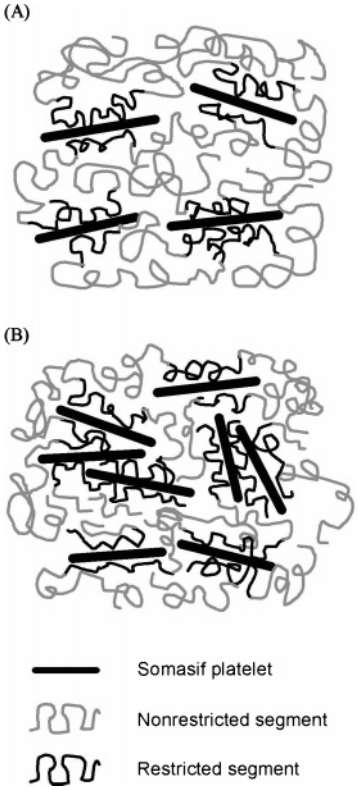

Figure 8. Schematic representation of PMA/Somasif nanocomposites with low (A) and high (B) Somasif content. PMA chains restricted due to their proximity to the Somasif surface, and nonrestricted chains are represented with black and gray lines, respectively.

Although ESR results point to a region of restricted polymer mobility in the interfacial region that is significantly separated from the bulk region, no distinct glass transition of the interfacial region was detected by DSC. This result can be rationalized by the difference in the frequency dependence of glass transitions in the bulk and interfacial regions.[36] According to a recent report, the difference in the glass transitions in the bulk and interfacial regions of poly(dimethylsiloxane) filled with silica nanoparticles increased with an increase in the frequency.[36] The relaxation time, τ_c, detected by DSC is $\approx$100 s, and the frequency, $\nu = 1/(2\pi\tau_c)$, is $\approx 2 \times 10^{-3}$ Hz.[37] On the other hand, the ESR frequency is $\approx 9 \times 10^9$ Hz (X-band). Therefore, the mobility in the interfacial region was detected by ESR and not by DSC.

The rigid layers of PMA at the clay surface are responsible for improved mechanical properties and better thermal and dimensional stabilities of matrix polymers. Moreover, the lower molecular mobility can inhibit the diffusion of oxygen and of unstable intermediates that can initiate degradation. This effect is not detected when the dispersion scale of the clay is larger than nanoscale: As seen in Figure 5B, the mobility of PMA in SP15 was significantly reduced compared with that in the COMP15, even though both samples contained the same amount of Somasif. In addition, the intensity of the slow component is significantly lower in COMP15 compared to SP15, 40% vs 76%. These results emphasize the important effect of the clay dispersion scale on polymer properties.

Thickness of Interfacial Regions. As seen in Figure 6, the relative intensity of the slow component in the ESR spectra of SP*n* nanocomposites increased with increasing Somasif content due to the larger rigid interfacial region. Moreover, the intensity ratio of the fast and slow components was almost constant above 390 K (Table 3). These results imply that the slow component above 390 K reflects the mobility in the interfacial region and

Table 4. Thickness of the Rigid Interface[a]

sample	D (nm)	t_{int} (nm)
SP03	67	15 ± 1.0
SP07	28	10 ± 0.5
SP15	12	5 ± 0.3

[a] D is the average distance between dispersed Somasif platelets, and t_{int} is the average thickness of the rigid interface.

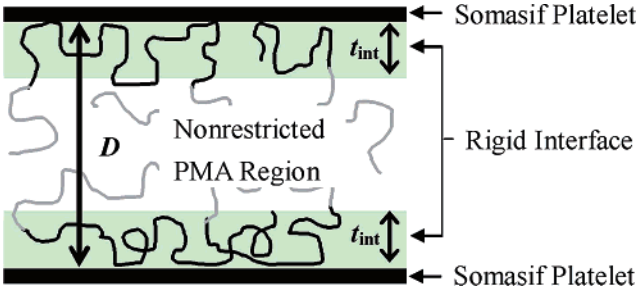

Figure 9. Average thickness of the polymer−clay interface, t_{int}, and the average distance between exfoliated clay platelets, D. See text.

correlates with the size of the interfacial region in the nanocomposites.

The average thickness of the interface, t_{int}, listed in Table 4 for SP03, SP07, and SP15 at 400 K was calculated from eq 1

$$t_{int} = (\%\ \text{slow})D/200 \quad (1)$$

where % slow is the intensity of the slow component (Table 3) and D is the average distance between exfoliated Somasif platelets in the nanocomposites, as shown in Figure 9.

D was calculated from eq 2

$$D = 2(1 - w)/d_{PMA}Sw \quad (2)$$

where w is the weight fraction of Somasif in the SPn sample, d_{PMA} is the density of the PMA, which was assumed to be equal to that of pure PMA, ≈1.2 g/cm^3,[38] and S is the specific surface area of Somasif platelets. S was calculated to be ≈800 m^2/g, using the density (2.6 g/cm^3) and the average lateral size (≈450 nm, both reported by the manufacturer) and the thickness (0.95 nm) deduced from XRD (Figure 1). In this calculation, the Somasif platelets were assumed to be disks with 450 nm diameter.

The estimated interfacial thickness is ≈5−15 nm, depending on Somasif content. The decrease in the average thickness of the interface with an increase in the Somasif content shown in Table 4 is most likely the result of some overlap of interfacial regions of different Somasif platelets, as shown in Figure 8B. As described above, the overlap of interfacial regions explained well the lower mobility in the interfacial region with an increase in the Somasif content.

Determination of the thickness of the rigid interfacial region is a major topic in composite materials. The interface thickness determined by NMR in silica-filled poly(ethyl acrylate) was ≈0.9 nm at 333 K; this value decreased slightly with increasing temperature but increased by a factor of 2 when the polymer chain had "anchor" points on the silica surface.[32] Fragiadakis et al. determined the interfacial thickness in silica-filled PDMS to be 2.1−2.4 nm by thermal stimulated depolarization currents (TSDC).[36] Zanten et al. studied the thermal behavior of ultrathin films of poly(2-vinylpiridine) on silicon oxide substrates using X-ray reflectivity and concluded that the length scale of the rigid interface was on the order of the macromolecular size, ≈21 nm.[39] These reports suggest that the thickness of a rigid interface is sensitive to the specific interaction between the polymers and the solid surface.

Effect of Surfactants. Surfactants are known to enhance the miscibility between clays and polymers.[1,2] Jeschke et al. used the spin-label ESR method to show the high mobility of free tails of surfactants.[18] The present study is an attempt to examine directly the effect of surfactants on polymer mobility.

The comparison of MEEP15 and SP15 provides the opportunity to compare dynamics of the same polymer in the presence and in the absence of surfactant. As seen in Figure 3B, $2A_{zz}$ measured at 100 K for MEEP15 is slightly lower than that of the SP15, most likely because the surfactants act as a buffer and displace the polymer from the Somasif surface. Moreover, the surfactants inhibit direct attachment of TMC groups on the Somasif surface, which explains the lower relative intensity of the slow component in MEEP15 (48%) compared to SP15 (76%).

In contrast to the situation in PMA, the ESR spectrum of the MEEP15 sample showed a fast component even at 340 K (Figure 4C). On the other hand, the ES values of the slow component in MEEP15 and SP15 are nearly the same. These results can be explained by assuming that some PMA chains or chain segments in MEEP15 are in contact with the Somasif surface, as reflected in the ES of the slow component, and the mobility of *restricted* chains in MEEP15 is comparable to that in SP15. The percentage of the slow component in MEEP15 is however much lower than in SP15, 48 vs 76 (Table 3). Analysis of the ESR spectra leads therefore to the conclusion that the surfactants have reduced, but not eliminated, the interaction between the polymer and the Somasif surface and have enhanced the mobility of intercalated PMA chains.

Conclusions

The structure and polymer dynamics in nanocomposites consisting of poly(methyl acrylate) (PMA) and synthetic fluoromica (Somasif) as the inorganic component were studied by X-ray diffraction (XRD), ESR spin-label technique, and differential scanning calorimetry (DSC). The polymer was modified by attachment of nitroxide and trimethylammonium chloride (TMC) groups (≈1 mol %). The TMC moieties act as anchoring groups and allow the preparation of exfoliated nanocomposites (SPn samples) even in the absence of surfactants.

The dynamics of PMA was studied in the nanocomposites and in modified PMA/clay nanocomposites prepared in the presence of surfactants (MEEPn), where n is the clay content. Structural data from XRD were combined with ESR results in order to assess the extent and intensity of polymer−clay interactions at the interface.

The mobility of PMA chains in the SPn nanocomposites was constrained due to the interactions between the PMA and Somasif in the interface region; the average thickness of the rigid interface was estimated to be in the range 5−15 nm by deconvolution of ESR spectra measured as a function of temperature into slow (S) and fast (F) components. The average thickness tended to decrease with increasing Somasif content, most likely because of overlap between Somasif platelets.

The influence of the surfactant on PMA mobility was also studied. In the MEEPn nanocomposites prepared in the presence of surfactants, ESR spectra allowed the detection of a small population of chain segments at the clay interface with dynamics similar to that in the SPn nanocomposites and additional chains with enhanced mobility.

Acknowledgment. This study was supported by the Polymers Program of the National Science Foundation. The authors

CDV

thank CO-OP Chemical, Japan, for the gift of the Somasif and MEE samples. The authors are also grateful to Dr. K. Yamamoto of the Nagoya Institute of Technology, Japan, for the GPC data, Dr. M. V. Motyakin for his help with the simulations, and Dr. J. Pilar of Academy of Science of the Czech Republic for valuable discussions. We are grateful to the two reviewers for their careful reading of the manuscript and helpful criticism.

References and Notes

(1) Pinnavaia, T. J.; Beall, G. W. *Polymer-Clay Nanocomposites*; Wiley & Sons: London, UK, 2000.
(2) Ajayan, P. M.; Schadler, L. S.; Braun, P. V. *Nanocomposite Science and Technology*; Wiley-VCH: Weinheim, Germany, 2004.
(3) Tyan, H.; Liu, Y.; Wei, K. *Chem. Mater.* **1999**, *11*, 1942.
(4) Agag, T.; Koga, T.; Takeichi, T. *Polymer* **2001**, *42*, 3399.
(5) Vyazovkin, S.; Dranca, I.; Fan, X.; Advincula, R. *J. Phys. Chem. B* **2004**, *108*, 11672.
(6) Vyazovkin, S.; Dranca, I. *J. Phys. Chem. B* **2004**, *108*, 11981.
(7) Huang, J.; Zhu, Z.; Yin, J.; Qian, X.; Sun, Y. *Polymer* **2001**, *42*, 873.
(8) Lu, H.; Nutt, S. *Macromolecules* **2003**, *36*, 4010.
(9) Tran, T. A.; Saïd, S.; Grohens, Y. *Macromolecules* **2005**, *38*, 3867.
(10) Vaia, R. V.; Jandt, K. D.; Giannelis, E. P. *Chem. Mater.* **1996**, *8*, 2628.
(11) Weimer, M. W.; Chen, H.; Giannelis, E. P.; Sogah, D. Y. *J. Am. Chem. Soc.* **1999**, *121*, 1615.
(12) Chen, H. W.; Chiu, C. Y.; Chang, F. C. *J. Polym. Sci., Part B: Polym. Phys.* **2002**, *40*, 1342.
(13) Liu, T.; Lim, K. P.; Tjiu, W. C.; Pramoda, K. P.; Chen, Z.-K. *Polymer* **2003**, *44*, 3529.
(14) Lee, Y.-H.; Bur, A. J.; Roth, S. C.; Start, P. R. *Macromolecules* **2005**, *38*, 3828.
(15) Liu, X.; Wu, Q. *Polymer* **2001**, *42*, 10013.
(16) Chen, J. S.; Poliks, M. D.; Ober, C. K.; Zhang, Y. M.; Wiesner, U.; Giannelis, E. *Polymer* **2002**, *43*, 4895.
(17) Shi, H. Z.; Lan, T.; Pinnavaia, T. J. *Chem. Mater.* **1996**, *8*, 1584.
(18) Jeschke, G.; Panek, G.; Schleidt, S.; Jonas, U. *Polym. Eng. Sci.* **2004**, *44*, 1112.
(19) Finnigan, B.; Jack, K.; Campbell, K.; Halley, P.; Truss, R.; Casey, P.; Cookson, D.; King, S.; Martin, D. *Macromolecules* **2005**, *38*, 7386.
(20) Chu, L.; Anderson, S. K.; Harris, J. D.; Beach, M. W.; Morgan, A. B. *Polymer* **2004**, *45*, 4051.
(21) Schneider, D. J.; Freed, J. H. In *Biological Magnetic Resonance;* Berliner, L. J., Reuben, J., Eds.; Plenum: New York, 1989; Vol. 8, p 1.
(22) Budil, D. E.; Lee, S.; Saxena, S.; Freed, J. H. *J. Magn. Reson. A* **1996**, *120*, 155.
(23) Miwa, Y.; Sugino, Y.; Yamamoto, K.; Tanabe, T.; Sakaguchi, M.; Sakai, M.; Shimada, S. *Macromolecules* **2004**, *37*, 6061.
(24) Maiti, P. *Langmuir* **2003**, *19*, 5502.
(25) Chen, B.; Evans, J. R. *J. Phys. Chem. B* **2004**, *108*, 14986.
(26) Griffith, O. H.; Jost, P. C. In Berliner, L. J., Ed.; *Spin Labeling Theory and Applications*; Academic Press: New York, 1976; p 453.
(27) Griffith, O. H.; Dehlinger, P. J.; Van, S. P. *J. Membr. Biol.* **1974**, *15*, 159.
(28) Shimada, S.; Maruta, A.; Yamamoto, K. *Polym. J.* **2000**, *32*, 1038.
(29) Shimada, S.; Sugimoto, A.; Kawaguchi, M. *Polymer* **1997**, *38*, 2251.
(30) Kutsumizu, S.; Schlick, S. *J. Mol. Struct.* **2005**, *739*, 191.
(31) Gardebien, F.; Gaudel-Siri, A.; Brédas, J.-L.; Lazzaroni, R. *J. Phys. Chem. B* **2004**, *108*, 10678.
(32) Berriot, J.; Lequeux, F.; Monnerie, L.; Montes, H.; Long, D.; Sotta, P. *J. Non-Cryst. Solid.* **2002**, *307−310*, 719.
(33) Mansfield, K. F.; Theodorou, D. N. *Macromolecules* **1989**, *22*, 3143.
(34) Miwa, Y.; Schlick, S., unpublished results.
(35) Brik, M. E.; Titman, J. J.; Bayle, J. P.; Judeinstein, P. *J. Polym. Sci., Part B: Polym. Phys.* **1996**, *34*, 2533.
(36) Fragiadakis, D.; Pissis, P, Bokobza, L. *Polymer* **2005**, *46*, 6001.
(37) Santangelo, P. G.; Roland, C. M. *Macromolecules* **1998**, *31*, 4581.
(38) Burgess, W. H.; Hopfenberg, H. B.; Stannett, V. T. *J. Macromol. Sci., Phys.* **1971**, *1*, 23.
(39) van Zanten, J. H.; Wallace, W. E.; Wu, W. L. *Phys. Rev. E* **1996**, *53*, R2053.

MA0600963